Electronic Supplementary Material (ESI) for CrystEngComm.


# SUPPLEMENTARY INFORMATION

## Crystallization Behavior of Citric Acid Based on Solution Speciation and Growth Kinetics

Estevao G. J. Macaringue,[a,b] Si Li,[a,b] Mengya Li, [a,b] Junbo Gong,[*,a,b,c] and Weiwei Tang[*,a,b,c]

[a] *State Key Laboratory of Chemical Engineering, School of Chemical Engineering and Technology, Tianjin University, Tianjin 300072, People's Republic of China*

[b] *The Co-Innovation Center of Chemistry and Chemical Engineering of Tianjin, Tianjin University, Tianjin 300072, People's Republic of China*

[c] *Tianjin Key Laboratory Modern Drug Delivery and High Efficiency, Tianjin university, Tianjin 300072, People's Republic of China*

Corresponding Authors: **jonbo_gong@tju.edu.cn (J. Gong)**; **wwtang@tju.edu.cn (W. Tang)**

This supporting material includes additional data to that given or referred to in the main manuscript.

## Supplementary Method 1: Full interaction map calculations

The molecular interaction maps preferences on the surface of crystal structures of monohydrate (CSD refcode: CITRAC10 $P2_1/a$)[1] and anhydrous (CSD refcode: CITARC01 $P2_12_12_1)_2$ forms of CA were assessed using the program Mercury[3] as the 3D structure visualizer and the intermolecular crystal structure evaluator. The full interaction maps (regions around the molecules) are calculated where chemical probe groups are likely to be found, based on pre-extracted crystallographic and theoretical data on intermolecular nonbonded interactions (IsoStar).[4] The tool first identifies distinct functional groups in the molecules viewed, and ten relevant interaction data in IsoStar. Next it pulls together the group-based interaction data and takes into account the environmental effects of combinative factors and steric extrusion to create a full 3D picture of molecular interaction preferences.[5]

The calculation procedures presented here, followed the instructions given in the Mercury User Guide[5] and Wood *et al*.[6] The probes used are the same as those defined in the tool's default settings which serve as proxies to reflect molecular interaction preferences concerning to H-bond donors (blue) and H-bond acceptors (red). The contour levels defined as default were changed from 2, 4, and 6 (with increasing levels of opacity) to 0, 0, 6 (only contour with the highest level of opacity shown). The interaction maps for single molecules of the monohydrate and anhydrous forms of CA were acquired by choosing the related structure and calculating maps with a contour level 6. To calculate the interaction maps on the Bravais-Freidel-Donnay-Harker (BFDH), the molecular structure of the crystal of interest was selected and then the morphology was predicted and filled with molecules. After this step, the remaining procedures for the calculation of the interaction maps on the BFDH were the same as those applied for the isolated molecules. Finally, to calculate the interaction maps on the packed slices the molecule was selected and then a slicing that includes atoms in molecules whose centroid fit, was activated. For comparison proposes, the selected planes are those with the strongest interaction preferences according to the applied probe types – which are believed to be the fastest faces of both crystal forms.

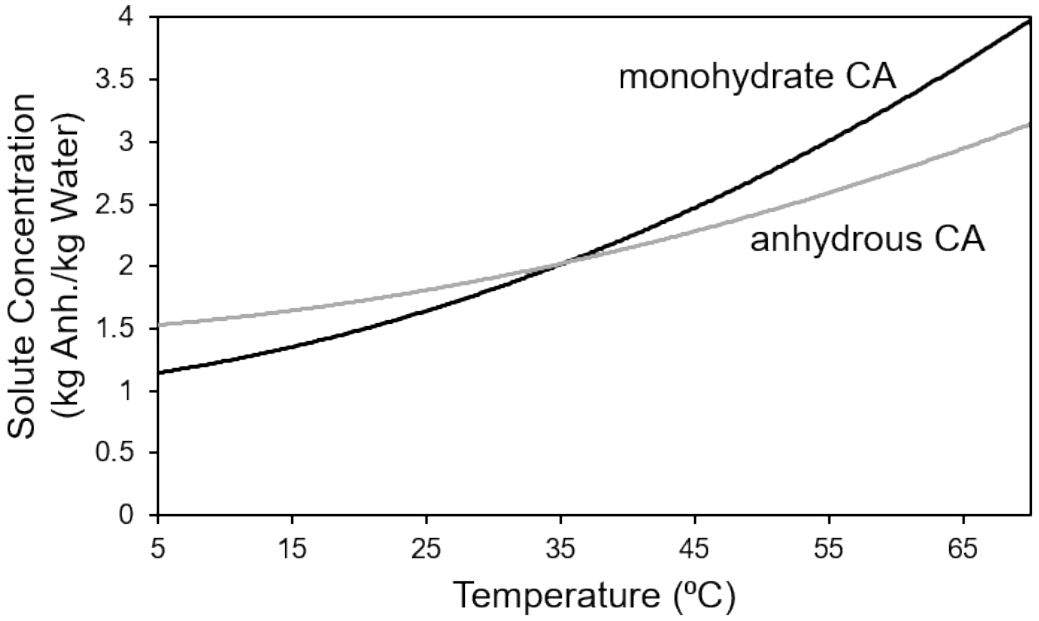


**Figure S1.** Solubility of citric acid (CA) in water (from A. Caillet *et al*.,).[7]

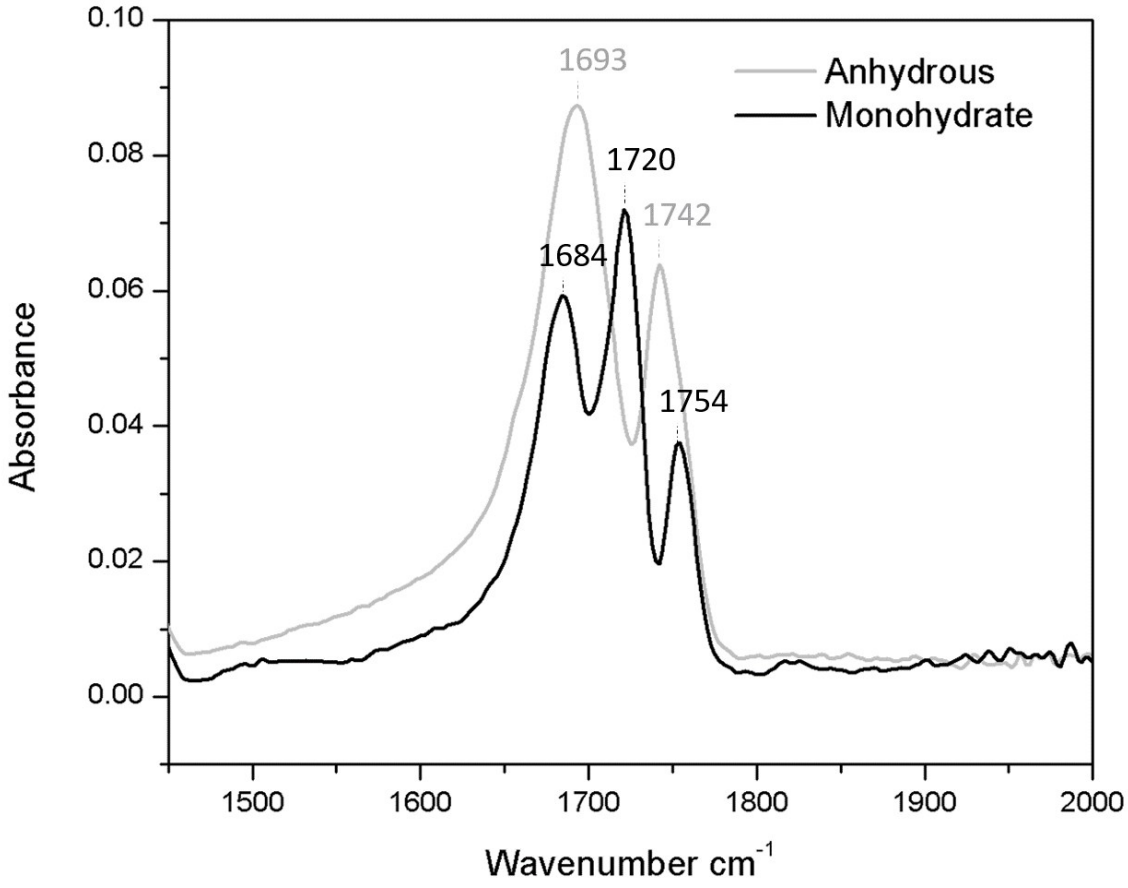


**Figure S2.** FTIR spectra displaying the distintion between the C=O stretching bands of anhydrous and monohydrate CA in the range of 1400-2000 $cm^{-1}$.

## Supplementary Note 1: Results from crystallization experiments.

In this section, we provide the data used to prepare the crystallization solutions and the particular results obtained in each experimental repetition. The illustration of crystallization outcomes given in Figure 1 of the main manuscript resulted from the compilation of results shown in Table S1.

**Table S1.** Results from the crystallization of CA in aqueous solutions (at different supersaturations and temperatures). For each set of conditions, the experiments were repeated at least 5 times. CAA indicates the appearance of a majority of CA anhydrous phase, and CAM expresses the predominance of CA monohydrate form.

| Crystallization temperature (°C) | Initial solute conc. (kg Anh./kg water) | Supersaturation ratio | Crystallization outcome | | |
|---|---|---|---|---|---|
| | | | CAA | CAM | Outcome |
| 15 | 2.19 | 1.34 | 5 | 0 | CAA |
| | 2.25 | 1.37 | 4 | 1 | CAA |
| | 2.49 | 1.52 | 5 | 0 | CAA |
| | 2.87 | 1.75 | 0 | 5 | CAM |
| 25 | 2.06 | 1.16 | 5 | 0 | CAA |
| | 2.21 | 1.24 | 5 | 0 | CAA |
| | 2.39 | 1.34 | 5 | 0 | CAA |
| | 2.44 | 1.37 | 5 | 0 | CAA |
| | 2.71 | 1.52 | 2 | 3 | CAM |
| | 3.12 | 1.75 | 0 | 5 | CAM |
| 40 | 2.55 | 1.19 | 5 | 0 | CAA |
| | 2.65 | 1.24 | 5 | 0 | CAA |
| | 2.78 | 1.3 | 5 | 0 | CAA |
| | 3.10 | 1.45 | 4 | 1 | CAA |
| | 3.45 | 1.61 | 5 | 0 | CAA |
| 45 | 2.73 | 1.19 | 4 | 1 | CAA |
| | 2.84 | 1.24 | 2 | 3 | CAM |
| | 2.98 | 1.3 | 5 | 0 | CAA |

| | | | | | |
|---|---|---|---|---|---|
| | 3.32 | 1.45 | 5 | 0 | CAA |
| | 3.69 | 1.61 | 5 | 0 | CAA |

## Supplementary Note 2: Crystal growth and growth dynamics monitored by polarizing microscopy.

The measurement of crystal growth was repeated in an independent experiment to ensure the accuracy of the results. Figure S3 and Figure FS4 show additional results related to the growth behavior of both forms of CA to support the results given in Figure 5 of the main manuscript.

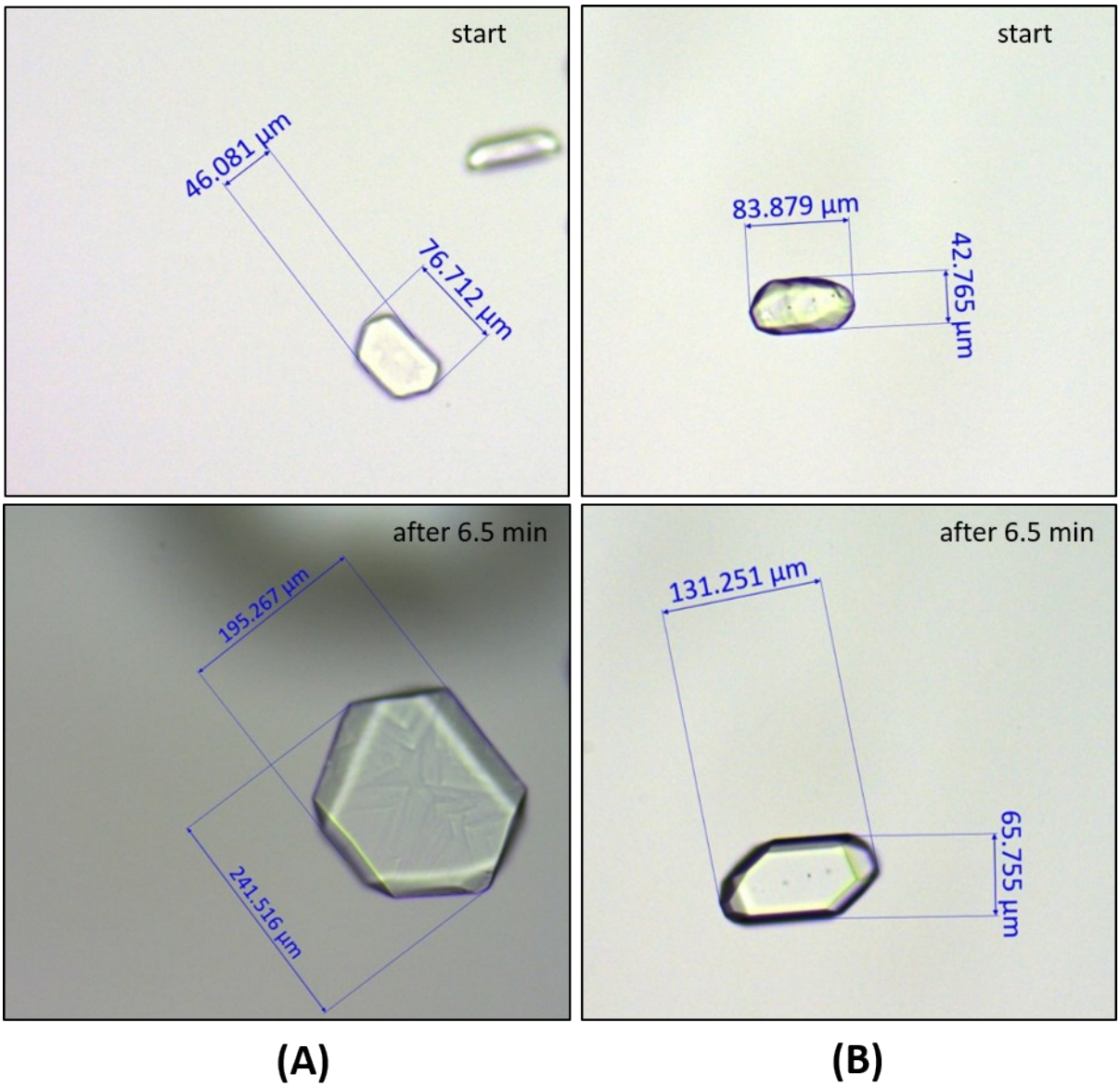


**Figure S3.** Additional data from in situ measurements of crystal growth of anhydrous (A) and monohydrate (B) CA. These images represent the morphologies at the beginning of the

experiment (right after the addition of the seeds into the solution, saturated at 40°C) and 6.5 minutes later.

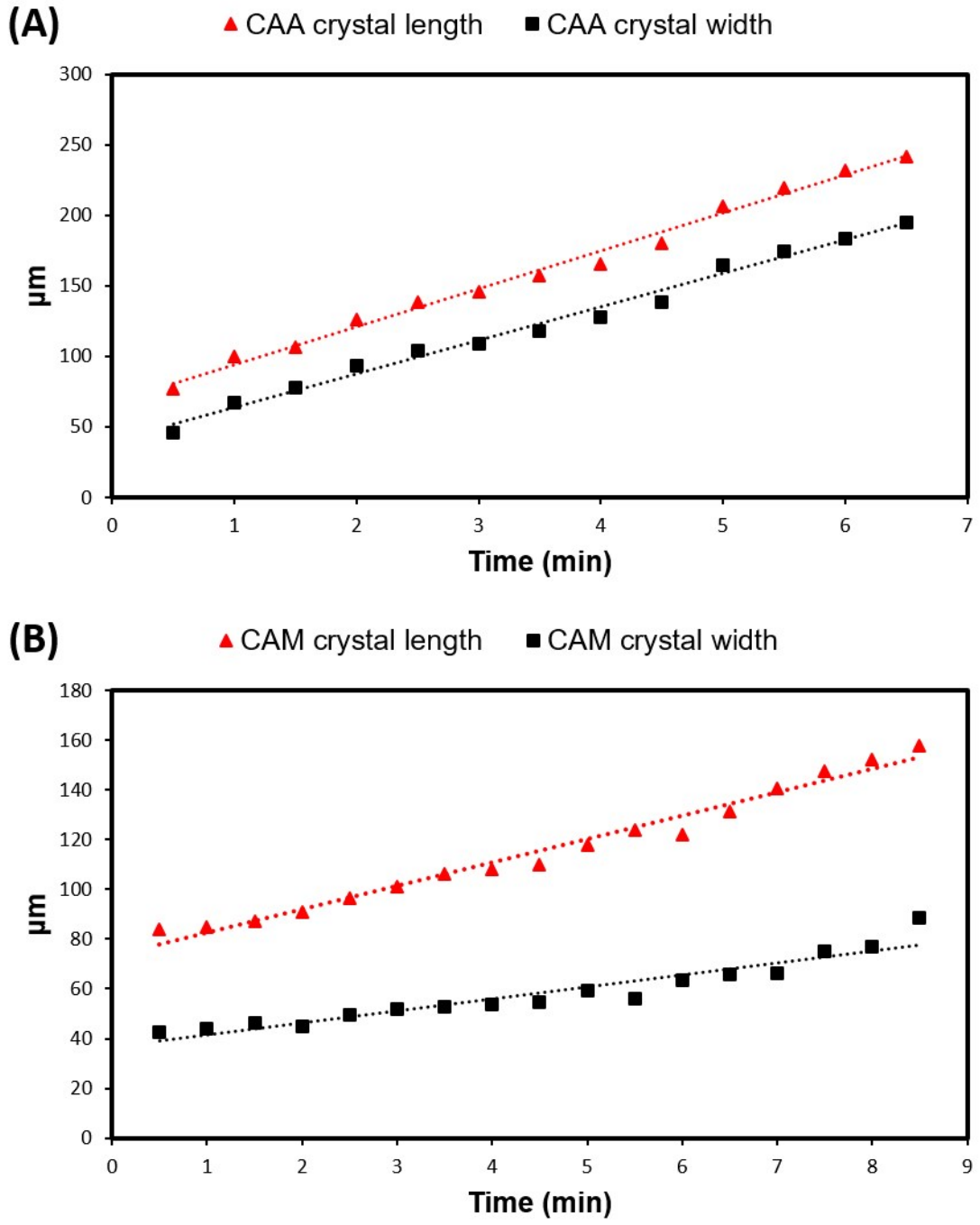


**Figure S4.** Growth dynamics of anhydrous (A) and monohydrate (B) phases. Pure red triangles and pure black squares correspond to data from the crystal length and width measurements, respectively.

## Supplementary Note 3: Preferential interactions of CA solvation and crystal growth

The kinetic advantage (higher nucleation or growth rates) has been suggested to explain the preferential crystallization of either metastable phases (in systems that obey the Ostwald's rule)[8,9-11] or stable phases (in systems that contradict the rule of stages)[12-16] at different crystallization conditions. Nevertheless, understanding the molecular dynamics involved in the nucleation and growth of CA that reinforce the unexpected appearance of the anhydrous phase at conditions that thermodynamically would favor the nucleation of the monohydrate can be of preeminent importance. This has been done by further investigating the nucleation and growth kinetics using a technique already established for identifying favorable interaction sites in crystalline materials.[17] The full interaction Mapping allows to assess how the crystal packing environment can satisfy the interactions of the functional groups of the molecule.[5] Different contour surfaces generated are applied to indicate how much likely an interaction is at a certain grid-point, while opacity levels are used to show the contour surfaces. The most opaque contour surfaces have the highest contour levels.[17]

In principle, the presence of water molecules in the structure of the monohydrate phase could make the equivalent comparison extremely hard. However, the conformation of the citric acid molecules and the hydrogen bond network within the lattice are different in the two structures.[18,19] This facilitated the comparison between the interaction maps generated from the two structures as different conformations resulted in distinguishable maps. In terms of the molecular structure of the two tricarboxylic molecules of CA, it is known that one of the terminal carboxyl groups of both molecules is an acceptor of intramolecular hydrogen bonding from the hydroxyl group[20] but it is only in the anhydrous form that this terminal carboxyl moiety is involved in the dimer type hydrogen bonding with a neighboring identical carboxylic group.[20,21]

The resulting molecular interaction maps show that both crystal structures of isolated CA molecules (Figure S5) have strong donor and acceptor capabilities around the carboxylic groups and have slightly similar geometrical distribution. However, it is exclusively in the terminal carboxylic group of anhydrous form involved in the cyclic dimer type hydrogen bonding that the interaction map peaks have a matching donor and acceptor atoms within

their contours. The remaining contacts in anhydrous and monohydrate forms are shown to have less hydrogen bonding propensity as all of the preferred donor interactions are not satisfied by contacts from neighboring molecules, only the center of the geometric location of the acceptor peaks coincide with the interacting atoms. This may give some advantages to the rate of self-assembly and growth of the anhydrous phase over monohydrate, thus, it is imperative to navigate further into the molecular cluster interaction mechanism in the context of crystal growth.

Figure S6 shows the interaction maps of the predicted monoclinic (a) and rhombic (b) prisms of anhydrous and monohydrate CA, respectively. The internal molecular packing of both forms of CA has been discussed in former studies[21,22,2,3] and the internal molecular arrangement of the growing crystals of anhydrous and monohydrate (Figure S7 and Figure S8) seems to agree well with the description given in the literature. However, what has not been reported is how the molecules are arranged on the surface of the growing crystals and how that can affect the nucleation and growth of both phases. In the anhydrous phase (Figure S6-A), the molecules seem to be arranged in a way that the carboxylic groups forming dimers with the neighboring molecules are pointed onto the surface of the growing crystals and their interaction map peaks are the strongest and coincide with the center of the neighboring donor and acceptor atoms. A monohydrate form exhibits a different molecular arrangement on the surface of the growing crystal (Figure S6-B). The interaction sites are slightly out of the crystal surfaces and have a weaker interaction maps peaks which in most cases do not match with the surrounding donor and acceptor atoms. As it has been described in the case of an isolated molecule of monohydrate (Figure S5-B), no interaction peaks are matching with donors of the nearest molecules. A comparison of the growing faces of one of the highest BFDH relative areas of both crystals (Figure S9) also vouches for the fact that the signal of the hydrogen bond interactions is stronger on the surface of the growing anhydrous phase and matches well with the donors and acceptors of the neighboring carboxylic groups than in the case of monohydrate. It is thus tempting to speculate that the rapid nucleation and growth kinetics of anhydrous over monohydrate crystals, can be correlated with the presence of two strong and attractive hydrogen bonding sites on the dimeric carboxylic groups of anhydrous phase as well as with the particular arrangement of the molecules of anhydrous CA on the crystal packing of the growing crystal - having the carboxylic moieties with the strongest and

cooperative hydrogen bonding interactions oriented onto the interface of the growing crystal. The former induces a quicker molecular self-association and the latter enhances the crystal growth.

Furthermore, if a closer look is paid into the graphics on Figures 5 of the main manuscript and Figure S4 it can be noted that the growth kinetics of crystal length and crystal width of anhydrous CA are closely related, that is, they grow at almost the same rate, however, in monohydrate CA the length seems to grow to a certain degree faster than the width. In Figure S11 the interaction maps were calculated around predicted BFDH structures and compared with morphologies of their related crystals. Our analyses indicate that the similarity of the growth rate of anhydrous phase in both length and width directions is associated to the equitable hydrogen bond interaction strength of the carboxylic groups located along with the faces of the crystal, while in the monohydrate phase the relatively fast elongation in the length direction seems to be generated by the preferential higher concentration of stronger interaction sites on the faces of that direction. It is thus believed that the selective growth kinetics on the crystal faces of the monohydrate can be correlated with differences in the strength of intermolecular interactions and may interfere in the overall growth rate of monohydrate over anhydrate.

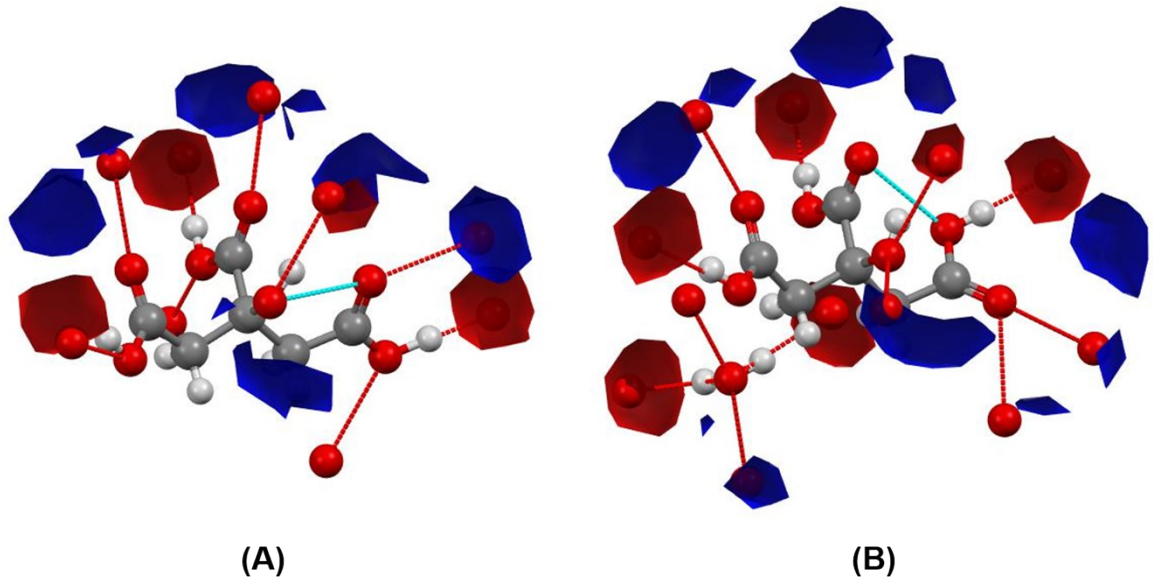


**Figure S5.** Preferential interaction sites for single molecular entities of anhydrous and monohydrate forms of CA. Domains for donor groups are shown in blue and for acceptor classes in red. The hydrogen bonds are shown to facilitate the identification of cooperative and non-cooperative interaction sites.

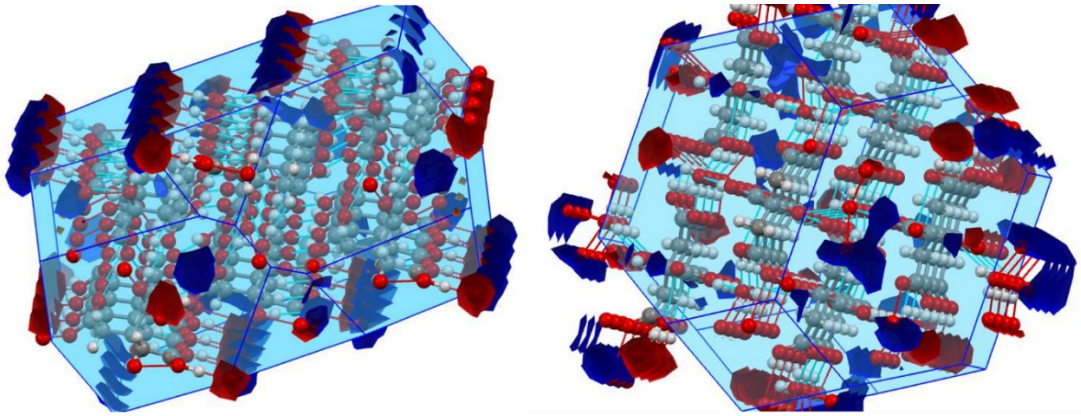


**Figure FS6.** Interaction maps on the surface of growing crystal structures of BFDH morphologies (packed with molecular clusters) of anhydrous (A) and monohydrate (B) forms of CA.

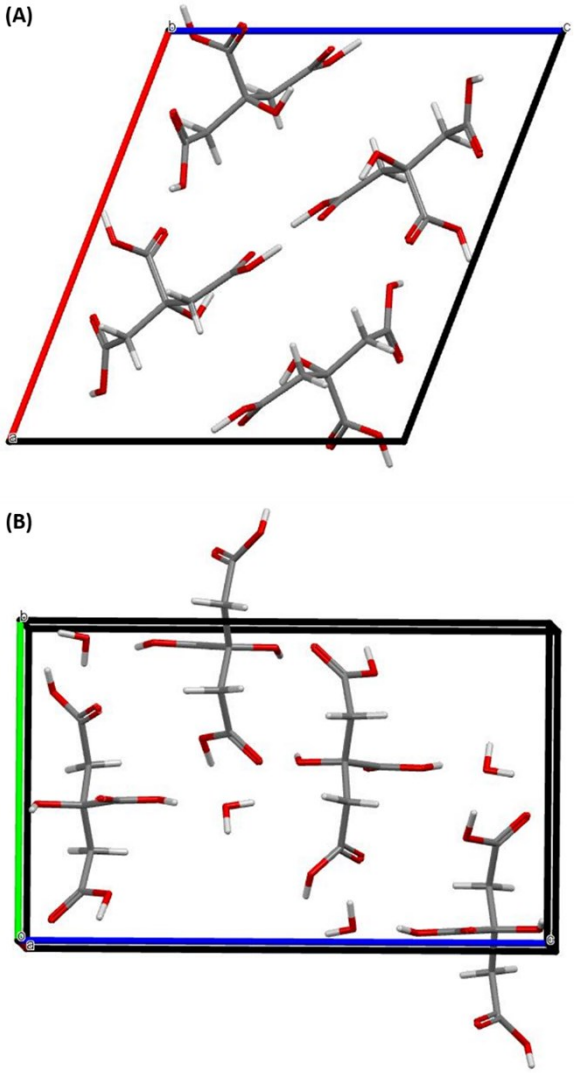


**Figure S7.** Molecular organization in the crystal structures of anhydrous (A) and monohydrate (B) forms.

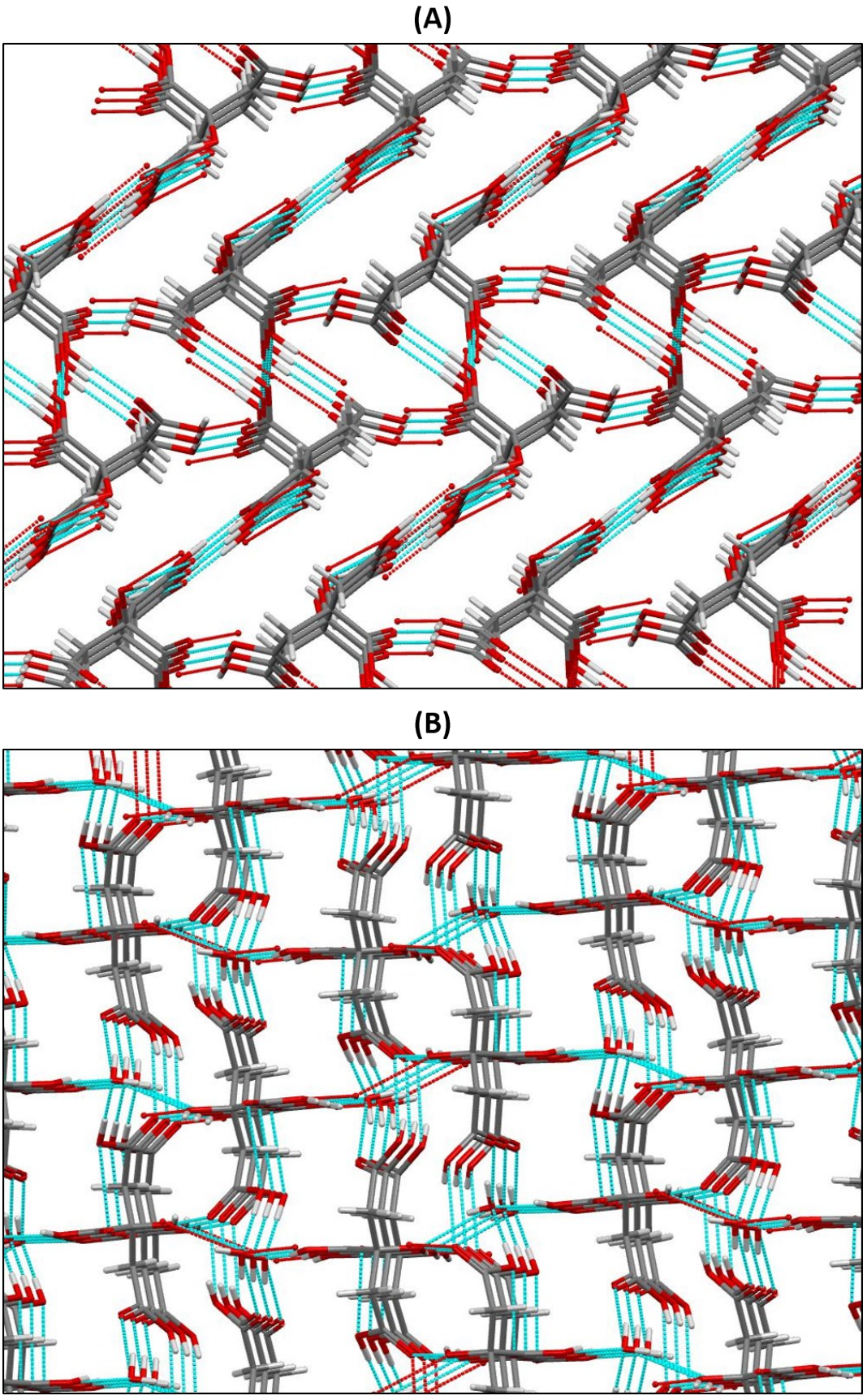


**Figure S8.** Molecular organization in the crystal structures of anhydrous (A) and monohydrate (B) forms. The dashed blue lines represent the possible hydrogen bonds in both structures.

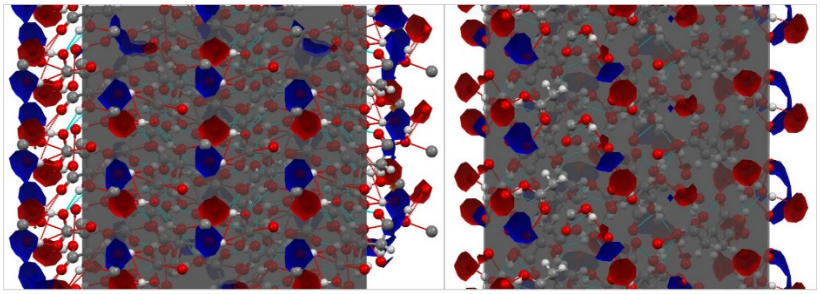


**Figure S9.** Comparison of interaction sites for the (00-1) and (01-1) surfaces of anhydrous (A) and monohydrate (B) crystals. These surfaces are among those with the highest BFDH relative areas per each crystal shape.

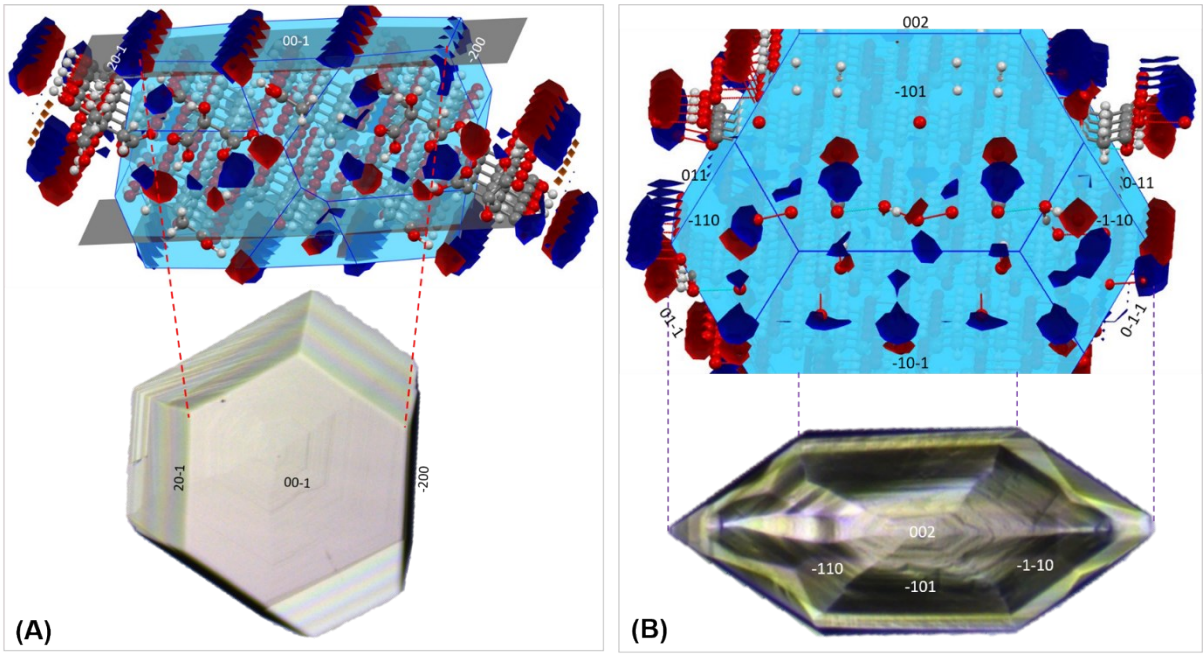


**Figure S10.** Interaction maps calculated around the predicted BFDH structures of anhydrous (A) and monohydrate (B) forms compared with morphologies of their related CA crystals.

**Influence of solution concentration on pH at 25°C.** Table S2 and Figure S11 give the trend of the pH with the increase of the CA solution concentration.

**Table S2. The** pH of anhydrous CA in water as a function of concentration at 25°C.

| **Conc. (M)** | 0.05 | 0.1 | 0.2 | 0.4 | 0.8 | 1.6 | 3.2 | 6.4 | 10.65 | 11.39 |
|---|---|---|---|---|---|---|---|---|---|---|
| **pH** | 2.23 | 2.10 | 1.93 | 1.68 | 1.67 | 1.63 | 1.29 | 1.0 | 0.51 | 0.21 |

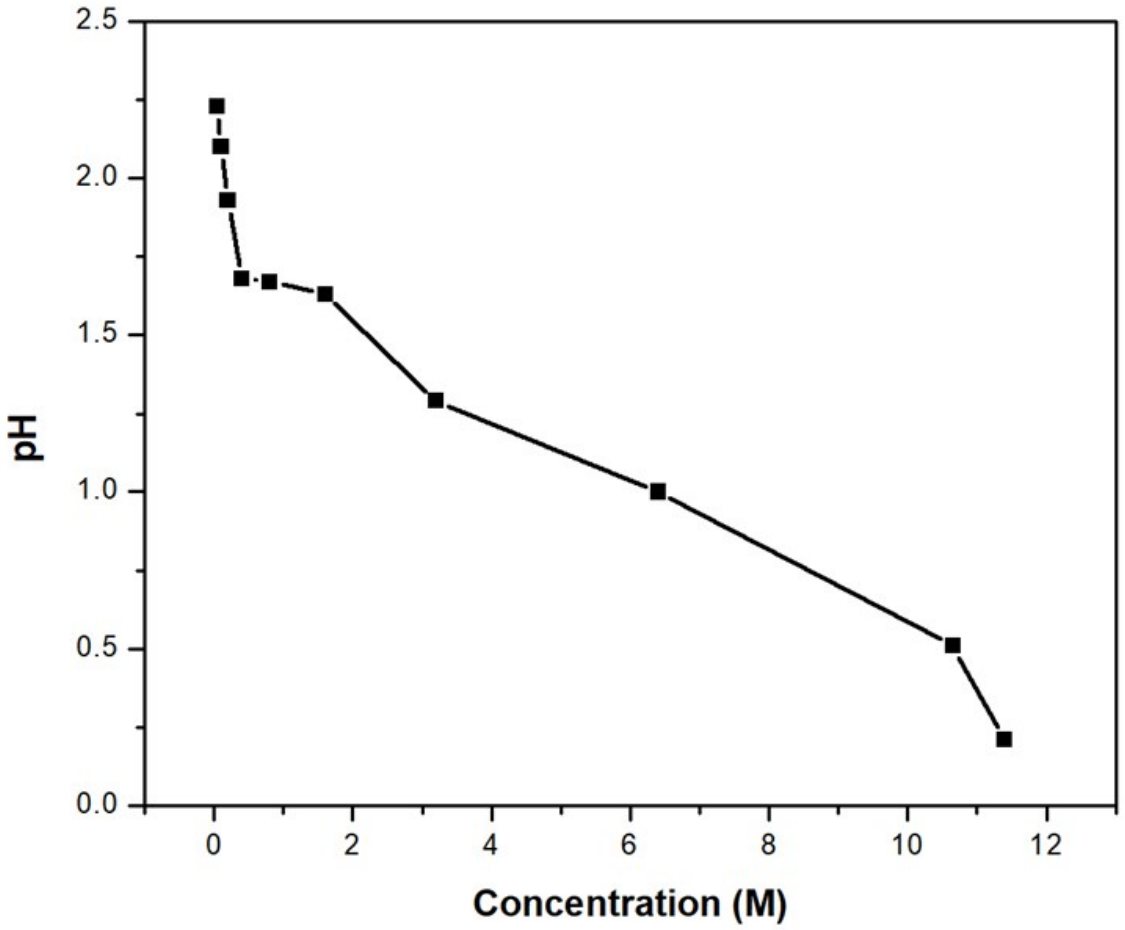


**Figure S11.** The trend of CA pH as a function of anhydrous phase concentration at 25°C.

## Supplementary Note 4: Temperature and concentration effect on the solution speciation of CA.

The influence of concentration and temperature on the ionization diagrams of CA was accessed by taking into account the correlation between solution concentration and pH, and the links between the temperature and $pK_a$ (which was used to correct the model parameters

that were introduced on the HySS software[23] to include the temperature effect on the solution speciation of CA), respectively. The $pK_a$ values determined at various temperatures (25-50°C) by Saeeduddin *et al*.[24] were interpolated to get the additional value of pka at 15°C that was not covered by their study (Figure S12).

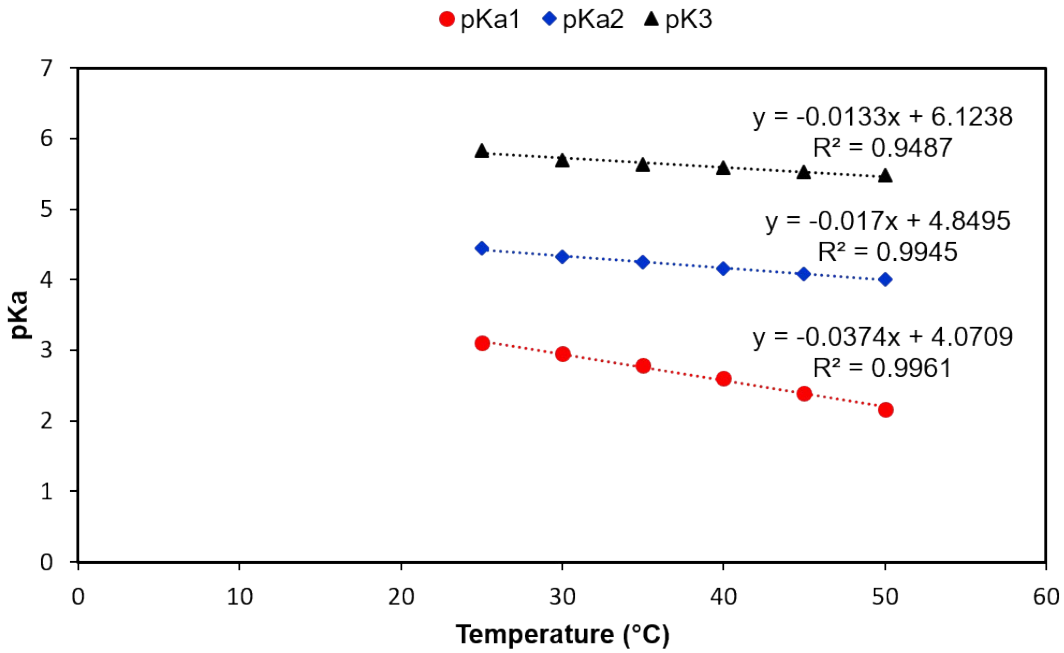


**Figure S12.** $pK_a$ values of CA in the function of temperature. The trending equations were used to interpolate the data given in Saeeduddin *et al*.[24] work to obtain the $pK_a$ value at 15°C.

**Table S3.** $pK_a$ values with their related model parameters used to investigate the influence of temperature on the solution speciation of anhydrous CA by the HySS software[23]. The $pK_a$ data from 25 to 45°C was obtained from a former study[24] and the value at 15°C was found by doing the interpolation given in Figure S12.

| T (C) | pKa1 | pKa2 | pK3 | β11 | β12 | β13 |
|---|---|---|---|---|---|---|
| 15 | 3.510 | 4.595 | 5.924 | 5.924 | 10.519 | 14.029 |
| 25 | 3.112 | 4.442 | 5.836 | 5.836 | 10.278 | 13.390 |
| 35 | 2.781 | 4.247 | 5.637 | 5.637 | 9.884 | 12.665 |
| 40 | 2.598 | 4.163 | 5.582 | 5.582 | 9.745 | 12.343 |
| 45 | 2.394 | 4.084 | 5.523 | 5.523 | 9.607 | 12.001 |

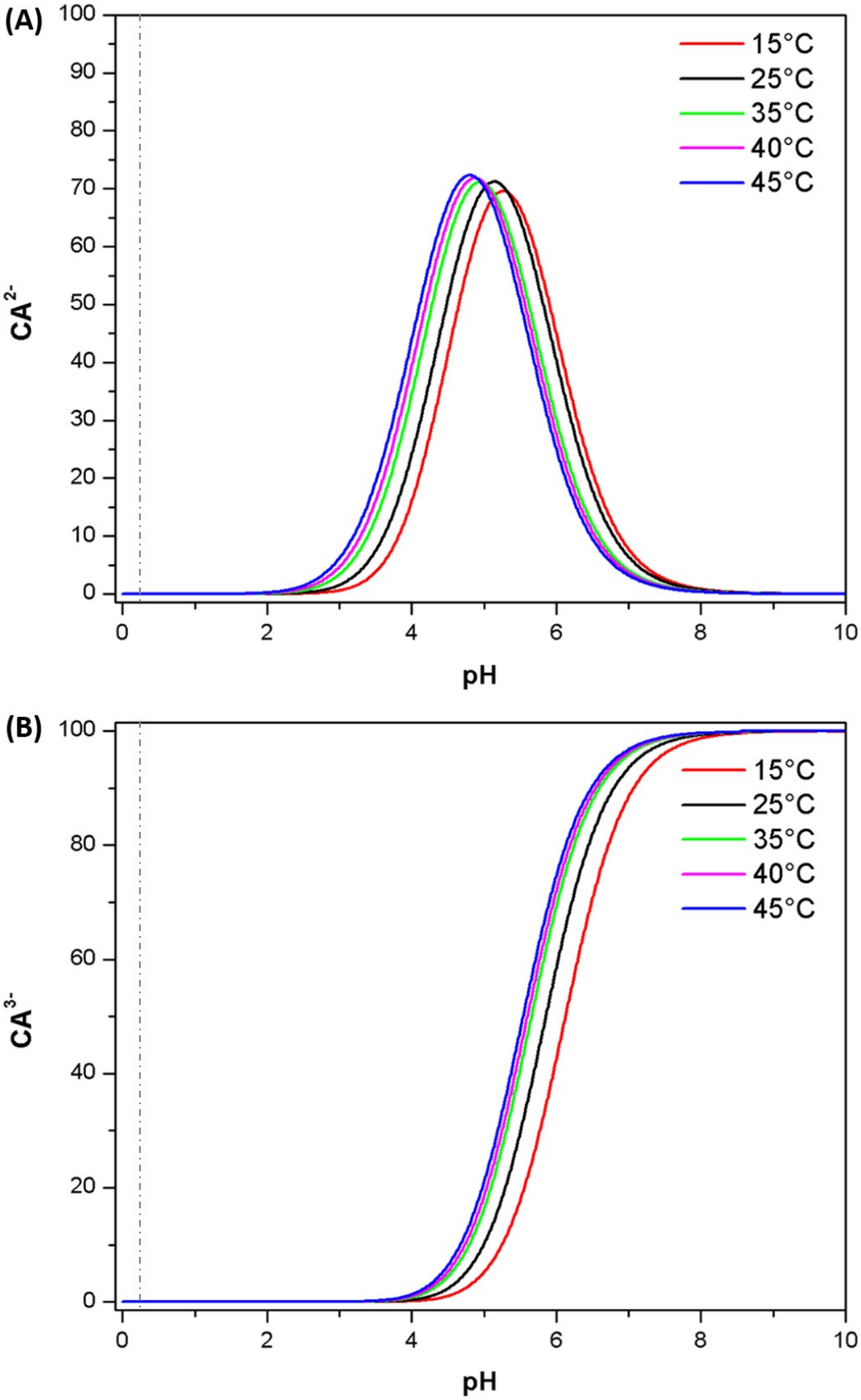


**Figure S13.** Solution speciation of CA in water from the second (A) and third (B) dissociation steps.

**References**


(1) J. P. Glusker, J. A. Minkin, and A. L. Patterson, *Acta Crystallographica Section B Structural Crystallography and Crystal Chemistry,* 1969, *25(6), 1066–1072.*

(2) G. Roelofsen, J. A. Kanters, Cryst. Struct. Commun. (1972), 1, 23-26.

(3) C. F. Macrae, I. J. Bruno, J. A. Chisholm, P. R. Edgington, P. McCabe, E. Pidcock, P. A. Wood, *Journal of Applied Crystallography,* 2008, *41(2), 466–470.*

(4) I. J. Bruno, J. C. Cole, J. P. M. Lommerse, R. S. Rowland, R. Taylor and M. L. Verdonk, *Journal of Computer-Aided Molecular Design,* 1997, *11(6), 525–537.*

(5) Mercury User Guide and Tutorials, 2019 CSD Release Update 3, Copyright © 2019 Cambridge Crystallographic Data Centre.

(6) P. A. Wood, T. S. G. Olsson, J. C. Cole, S. J. Cottrell, N. Feeder, P. T. A. Galek, E. Pidcock, *CrystEngComm,* 2013, *15(1), 65–72.*

(7) A. Caillet, F. Puel, and G. Fevotte, *International Journal of Pharmaceutics,* 2006, *307(2), 201–208.*

(8) M. Kitamura, *Journal of Crystal Growth,* 1989, *96(3), 541–546.*

(9) A. Keller, M. Hikosaka, S. Rastogi, A. Toda, P. J. Barham and G. Goldbeck-Wood, *Journal of Materials Science,* 1994, *29(10), 2579–2604.*

(10) M. Kitamura and T. Ishizu, *Journal of Crystal Growth,* 2000, *209(1), 138–145.*

(11) C. Desgranges and J. Delhommelle, *Journal of the American Chemical Society,* 2006, *128(32), 10368–10369.*

(12) J. F. B. Black, R. J. Davey, R. J. Gowers and A. Yeoh, *CrystEngComm,* 2015, *17(28), 5149–5142.*

(13) S. Gracin, and Å. C. Rasmuson, *Crystal Growth & Design,* 2004, *4(5), 1013-1023.*

(14) G. M. Maggioni, L. Bezinge and M. Mazzotti, *Crystal Growth & Design,* 2017, *17(12), 6703–6711.*

(15) M. Svärd, F. L. Nordström, E.-M. Hoffmann, B. Aziz, and Å. C. Rasmuson, *CrystEngComm,* 2013, *15(25), 5020.*

(16) K. Sato and R. Boistelle, *Journal of Crystal Growth,* 1984, *66(2), 441–450.*

(17) P. A. Wood, T. S. G. Olsson, J. C. Cole, S. J. Cottrell, N. Feeder, P. T. A. Galek, E. Pidcock, *CrystEngComm,* 2013, *15(1), 65–72.*

(18) C. F. Macrae, I. J. Bruno, J. A. Chisholm, P. R. Edgington, P. McCabe, E. Pidcock, P. A. Wood, *Journal of Applied Crystallography,* 2008, *41(2), 466–470.*

(19) A. Lafontaine, M. Sanselme, Y. Cartigny, P. Cardinael and G. Coquerel, *Journal of Thermal Analysis and Calorimetry,* 2012, *112(1), 307–315.*

(20) G. Roelofsen, J. A. Kanters, Cryst. Struct. Commun. (1972), 1, 23-26.

(21) A. Lafontaine, M. Sanselme, Y. Cartigny, P. Cardinael and G. Coquerel, *Journal of Thermal Analysis and Calorimetry,* 2012, *112(1), 307–315.*

(22) C. E. Nordman, A. S. Weldon and A. L. Patterson, *Acta Crystallographica,* 1960, *13(5), 418–426.*

(23) L. Alderighi, P. Gans, A. Ienco, D. Peters, A. Sabatini and A. Vacca, *Coordination Chemistry Reviews,* 1999, *184(1), 311–318.*

(24) A. W. k. Saeeduddin, Khanzada and A.T. Mufti. *Jour. Chem. Soc.,* **1996,** *Pak. Vol. 18, No. 2.*